# Deterministic Smoluchowski-Feynman ratchets driven by chaotic noise

Lock Yue Chew*

*Division of Physics and Applied Physics, School of Physical and Mathematical Sciences, Nanyang Technological University, 21 Nanyang Link, Singapore 637371*

(Received 19 August 2011; revised manuscript received 23 November 2011; published 23 January 2012)

We have elucidated the effect of statistical asymmetry on the directed current in Smoluchowski-Feynman ratchets driven by chaotic noise. Based on the inhomogeneous Smoluchowski equation and its generalized version, we arrive at analytical expressions of the directed current that includes a source term. The source term indicates that statistical asymmetry can drive the system further away from thermodynamic equilibrium, as exemplified by the constant flashing, the state-dependent, and the tilted deterministic Smoluchowski-Feynman ratchets, with the consequence of an enhancement in the directed current.

DOI: 10.1103/PhysRevE.85.016212 PACS number(s): 05.45.−a, 05.40.−a, 05.60.−k, 02.50.−r

## I. INTRODUCTION

Brownian ratchet is a useful paradigm for the basic understanding of thermodynamic systems driven far away from equilibrium [1]. As such, it has served as a useful conceptual framework for the construction of biophysical models for the locomotion of protein motors [2,3], as well as more complex biochemical and catalytic reactions [4,5]. Currently, ideas from Brownian ratchet are being actively considered in systems where thermal or nonthermal noise are being exploited for applications such as molecular pumps [6,7], sieves [8–11], and diodes [12,13]. These devices, whose operations are based on the symmetry breaking principle in Brownian ratchets, control the flow of nanoscale molecules by directing their transport in a noisy environment to achieve a specific function. While there are many considerations on the design of these novel devices, the situation where the ratchets are being driven by chaotic noise needs to be thoroughly investigated. This has motivated us to examine the behavior of ratchets subjected to chaotic noise. Ratchets driven by chaotic noise are deterministic ratchets [14–20] because chaotic noise originates from deterministic systems. Since we will be restricting our studies to the overdamped regime, our ratchets belong to the class of overdamped deterministic ratchets [21,22], instead of the inertia [23–25] or the Hamiltonian deterministic ratchets [26,27]. Moreover, by focusing our investigation on chaotic noise with broken statistical symmetry, our ratchets are also known as the asymmetrically tilted ratchets [28–31].

It is well known that directed transport occurs in ratchet systems when all the symmetries within the systems are broken [1,26,32,33]. This is known as Curie's principle. Indeed, the transport comes in the form of directed current, which provides a mechanism for particle separation. For ratchet systems, the symmetry can appear either explicitly or implicitly in the form of supersymmetry, within the ratchet potential or the driving noise. The symmetry can also appear in the form of detailed balance. In this paper, we have introduced asymmetry into our potential such that they are spatially asymmetric without any hidden symmetries. Similar consideration applies to the chaotic noise through the breaking of statistical symmetry. If detailed balance symmetry is also broken within our ratchet systems, the presence of directed current is to be expected. Nonetheless, the key results of our paper is not on the occurrence of the directed current, but on the enhancement of its magnitude through the control of the concomitant influences of the resulting asymmetries and the driving of our systems away from thermodynamic equilibrium. Note that the forces we consider in our system have vanishing temporal and spatial ensemble averages.

Our approach, which is described in Sec. II, is based on the modification of a discrete-time map that has been proven to model the dynamics of Brownian motion when the noise is white and obeys the Gaussian random process [34]. We have modified the map by considering chaotic noise instead of Gaussian noise, with the chaotic noise arises from the class of Tchebyscheff maps [35]. We have also extended the map by incorporating a space-dependent force field on the Brownian particle [28]. This extension has allowed us to examine the mechanism of chaotic transport and chaos-induced escape over potential barriers [36]. It has led us to investigate ratchets driven by chaotic noise both numerically and analytically. For directed transport to occur in our ratchet systems, we can employ chaotic noise that is colored [37,38] or statistically asymmetric [31,39] if the potential is spatially periodic and symmetric. It is the latter statistical property of the noise that is of interest in this paper. Consequently, we examine the effect of the statistical asymmetry of the noise on a Brownian particle in a free field numerically, as well as analytically by means of a set of Feynman graphs, in Sec. III of this paper. Then in Sec. IV, we go beyond our earlier treatment and observe the manner in which the transport of a Brownian particle is being controlled by adjusting the asymmetry of a spatially periodic potential, while the particle is subjected to chaotic noise, in a model that we termed the deterministic Smoluchowski-Feynman ratchet. In Sec. V, we proceed to consider the transport behavior of a constant flashing Smoluchowski-Feynman ratchet in chaotic noise, as well as a version that flashes dichotomously. In Sec. VI, we further generalize our discrete-time system to the case with state-dependent diffusion. This generalization allows us to model situations when the particle is subjected to chaotic noise with intensity that varies periodically in space. Our analysis on this scenario results in a generalized Smoluchowski equation with a source term, whose solution gives the directed current of a deterministic ratchet with a spatially periodic "chaotic" heat bath. As a specific illustration, we consider

*lockyue@ntu.edu.sg

 

the case of a spatially periodic and asymmetric potential force field, which gives rise to a state-dependent deterministic Smoluchowski-Feynman ratchet. In Sec. VII, we further apply our analytical results in Sec. VI to derive the directed current of a tilted deterministic Smoluchowski-Feynman ratchet driven by nonequilibrium chaotic forces. Finally, we give a general discussion on our results before concluding our paper in Sec. VIII.

In summary, the research in this paper has gone beyond our earlier work [28,35,36] by providing a systematic treatment on the effects of asymmetry in the potential on directed transport through various configurations of deterministic Smoluchowski-Feynman ratchets driven by chaotic noise. In particular, we have derived a Smoluchowski equation with a source term [Eq. (50) below] that generalizes over our earlier result in [28] by taking into account the spatial dependence of diffusion.

## II. THE QUASISTATIONARY KICKED PARTICLE MAP

Let us consider the following quasistationary kicked particle (QKP) map [28]:

$$F_{n+1} = G^{(N)}(F_n), \tag{1}$$

$$p_{n+1} = e^{-\gamma\tau} p_n - \frac{V'(x_n)}{\gamma}(1 - e^{-\gamma\tau}) + (\gamma\tau)^{1/2} s F_{n+1}, \tag{2}$$

$$x_{n+1} = x_n + \frac{1}{\gamma}(1 - e^{-\gamma\tau})p_n - \frac{V'(x_n)}{\gamma}\left[\tau + \frac{1}{\gamma}(e^{-\gamma\tau} - 1)\right]. \tag{3}$$

This map gives the discrete-time position $x_n$ and momentum $p_n$ of a viscous dragged particle of unit mass which is acted upon by a space dependent force $-V'(x_n) = -dV(x_n)/dx$, with $V(x)$ being the potential field. The particle is also being kicked periodically at a time interval $\tau$ by chaotic forces $(\gamma\tau)^{1/2} s F_{n+1}$, where $\gamma$ is the friction coefficient of the medium and $s$ controls the intensity of the chaotic noise. Note that $s = 2\sqrt{k_B T}$, with $T$ being the temperature and $k_B$ the Boltzmann constant. The variable $F_n$ is chaotic and arises from the class of Tchebyscheff maps $G^{(N)}$. Functionally, $G^{(N)} : [-1,1] \to [-1,1]$ and can be determined via the recurrence relation:

$$G^{(i+1)}(F) = 2F G^{(i)}(F) - G^{(i-1)}(F). \tag{4}$$

The first few Tchebyscheff maps are given by $G^{(0)}(F) = 1$, $G^{(1)}(F) = F$, $G^{(2)}(F) = 2F^2 - 1$, $G^{(3)}(F) = 4F^3 - 3F$, and $G^{(4)}(F) = 8F^4 - 8F^2 + 1$. However, only the nonlinear Tchebyscheff maps, that is, $N \geqslant 2$, is of interest to us as the iterates from these systems are ergodic and $\phi$ mixing [40] with a natural invariant density,

$$h(F) = \frac{1}{\pi\sqrt{1 - F^2}}, \tag{5}$$

which is independent of $N$. Moreover, by expressing them mathematically in an alternative form, which is

$$G^{(N)}(F) = \cos(N \cos^{-1} F), \tag{6}$$

it is possible to determine the higher-order correlation functions of the iterates of the Tchebyscheff maps [41] through

$$\begin{aligned}\langle F_{n_1} F_{n_2} \cdots F_{n_r} \rangle_N &= \int_{-1}^{1} dF_0 h(F_0) F_{n_1} F_{n_2} \cdots F_{n_r} \\ &= 2^{-r} \sum_{\sigma} \delta_K(\sigma_1 N^{n_1} + \cdots + \sigma_r N^{n_r}, 0),\end{aligned} \tag{7}$$

where $\langle\cdot\rangle$ denotes expectation with respect to $h(F)$ [Eq. (5)] and $\delta_K(i,j)$ is the Kronecker $\delta$ function. Note that $\sigma_j = \pm 1$. In particular, for $r = 1$ and 2, we have

$$\langle F_i \rangle_N = 0, \tag{8}$$

$$\langle F_i F_j \rangle_N = \tfrac{1}{2}\delta_K(i,j). \tag{9}$$

The higher-order correlations expressed by Eq. (7) define the statistical properties of the chaotic dynamics of the Tchebyscheff maps. An interesting example regards the odd-order maps. For these maps, where $N$ is odd, all odd higher-order correlations (i.e., $r$ odd) vanish [42]. Therefore, iterates from the odd-order Tchebyscheff maps obey a multivariate probability density that is symmetric, and fluctuations produced by them are said to be statistically symmetric [43]. On the other hand, such symmetry is absent in the even-order Tchebyscheff maps due to the presence of the odd higher-order correlations, and as a consequence, fluctuations generated by them are deemed to be statistically asymmetric [39]. The Tchebyscheff maps, being semiconjugated to the Bernoulli shifts with an alphabet of $N$ symbols, have a Lyapunov exponent of $\log N$. Thus, the variable of the Tchebyscheff maps corresponds, in the context of our physical model, to a fast chaotic degree of freedom from a nonequilibrium heat bath with a Kolmogorov-Sinai entropy of $\log N/\tau$ [44]. This effectively implies a faster convergence to stochasticity the higher the order of the Tchebyscheff maps when the time scale $\tau$ is fixed and small [45].

## III. DIFFUSIVE MOTION FROM CHAOTIC FLUCTUATIONS BY MEANS OF THE FEYNMAN's GRAPH APPROACH

First, let us consider the case of free field, that is, $V'(x) = 0$, in Eqs. (2) and (3). In [35], we have proved that the motion of the dissipated particle obeys the Gaussian diffusion process while it is being driven by chaotic dynamics from the class of Tchebyscheff maps. The proof was based on the Salem-Zygmund theorem, which establishes that $x_n$ converges weakly to the Gaussian diffusion process for arbitrary $\gamma$ and $\tau$ as $n \to \infty$. In this section, we continue to investigate the stochastic convergence of the particle's motion, especially on its asymptotic rate of convergence toward the Gaussian diffusive process. Our investigation is based on an approach similar to the summation of Feynman's graphs. The approach employs the fact that the higher-order correlations of iterates of the Tchebyscheff maps can be described by a set of graphs, which are composed of interesting structures known by the name of double $N$-ary forests and trees [41]. These structures give a pictorial view to the statistical components of the

chaotic fluctuations and will be very useful in obtaining the higher-order correlations of the quantity

$$x_{n+1} = (4D\tau)^{\frac{1}{2}} \sum_{i=1}^{n} c_i F_i, \tag{10}$$

through a set of "Feynman rules" [46]. Note that Eq. (10) results from an iterative solution of Eqs. (2) and (3), which leads to

$$x_{n+1} = \frac{p_0}{\gamma}(1 - e^{-(n+1)\gamma\tau}) + (4D\tau)^{\frac{1}{2}} \sum_{i=1}^{n} c_i F_i, \tag{11}$$

with $D = k_B T/\gamma$ and $c_i = 1 - e^{-(n-i+1)\gamma\tau}$. Equation (10) is obtained by ignoring the first term on the right of Eq. (11) since it is of no consequence in the asymptotic regime $n \to \infty$.

We determine the position distribution function of the particle by performing a Fourier transform on the characteristic function $\Gamma^{(N)}(k)$ of $x_{n+1}$,

$$P^{(N)}(x_{n+1}) = \frac{1}{2\pi} \int_{-\infty}^{\infty} dk\, \Gamma^{(N)}(k) e^{-ikx_{n+1}}, \tag{12}$$

with $\Gamma^{(N)}(k)$ defined as follows:

$$\Gamma^{(N)}(k) := \langle e^{ikx_{n+1}} \rangle_N = \sum_{r=0}^{\infty} \frac{(ik)^r}{r!} \langle x_{n+1}^r \rangle_N. \tag{13}$$

The term $\langle x_{n+1}^r \rangle_N$ in Eq. (13) can be expressed in the following manner based on Eqs. (7) and (10):

$$\langle x_{n+1}^r \rangle_N = (D\tau)^{\frac{r}{2}} \sum_{i_1=1}^{n} \cdots \sum_{i_r=1}^{n} \sum_{\sigma} c_{i_1} c_{i_2} \cdots c_{i_r} \delta_K \left( \sum_{j=1}^{r} \sigma_j N^{n_j}, 0 \right), \tag{14}$$

with the set of tuples $\sigma$ satisfying the diophantic equation $\sum_{j=1}^{r} \sigma_j N^{n_j} = 0$ (i.e., contributing to $\langle x_{n+1}^r \rangle_N$) corresponds to the set of double $N$-ary forests. Then, analogous to the perturbative calculation of propagators in quantum field theory with the set of Feynman's diagrams corresponding to the set of double $N$-ary forests [47], certain topological structures of the forests contribute more than others. This enables a perturbative expansion of $\Gamma^{(N)}(k)$ into an infinite series:

$$\Gamma^{(N)}(k) = \Gamma_0^{(N)}(k) + \Gamma_1^{(N)}(k) + \Gamma_2^{(N)}(k) + \cdots, \tag{15}$$

with each component having different degrees of significance, depending on their topological structures. For example, the most important structures are those that represent the zeroth-order contributions, which are known as the trivial double trees. All Tchebyscheff maps possess these structures. In fact, the trivial double trees correspond to the higher-order correlations of a Gaussian stochastic process. In this way, we can understand in a diagrammatic manner the link between the deterministic dynamics of Tchebyscheff maps and the stochastic Gaussian limit of the particle's motion. Indeed, by summing the set of Feynman's graphs based on these structures, we obtain the following zeroth-order characteristic function $\Gamma_0^{(N)}(k)$ of the particle:

$$\begin{aligned}\Gamma_0^{(N)}(k) &= 1 + \sum_{\alpha=1}^{\infty} \frac{(ik)^{2\alpha}}{(2\alpha)!} \bullet\!\!\!\vdots\, \alpha \\ &= \sum_{\alpha=0}^{\infty} \frac{(ik)^{2\alpha}}{(2\alpha)!} \left[ 2^{-2\alpha} \left( 4D\tau \right)^{\alpha} \frac{(2\alpha)!}{\alpha!} \left( \sum_{j=1}^{n} c_j^2 \right)^{\alpha} \right] \\ &= \exp\left( - D\tau \sum_{j=1}^{n} c_j^2 k^2 \right),\end{aligned} \tag{16}$$

where the number $\alpha$ beside the trivial double tree denotes the number of such tree in each summand. Thus, we observe that the "Feynman rules" translate the topological structure of the forests into formulas that contribute to the higher-order correlation of $x_{n+1}$. By performing a Fourier transform on Eq. (16), and noting that $\sum_{j=1}^{n} c_j^2 \approx n$ for $n \to \infty$, we obtain the zeroth-order probability distribution function of the particle:

$$P_0^{(N)}(x_{n+1}) = \frac{1}{\sqrt{4\pi Dn\tau}} \exp\left( - \frac{x_{n+1}^2}{4Dn\tau} \right), \tag{17}$$

which is a single-point Gaussian distribution of a normal diffusive process. It is important to note that the topological structures of the diagram tell us more. Through its direct relation with the Gaussian random process, it provides us with an intuitive notion that the multipoint distribution of the particle in the zeroth-order limit is a multivariate Gaussian distribution.

Then, as we move away from the zeroth-order limit by increasing $\tau$ [41,46], topological structures in the form of a tree with a fork, while the rest are trivial double binary trees, come into significance. The contribution of these forests are first order and occur only for $N = 2$, because for $N > 2$ the above diagrams are not solutions to the corresponding diophantic equations [41]. This structure symbolizes one of the statistical asymmetries of the fluctuations and is believed to be a topological representation of the source term in the inhomogeneous Smoluchowski equation derived in [28] and its generalized version given by Eq. (50) below. By performing the Feynman sum on these forests, we arrive at the following first-order characteristic function $\Gamma_1^{(2)}(k)$ of the particle:

$$\begin{aligned}\Gamma_1^{(2)}(k) &= \sum_{\alpha=1}^{\infty} \frac{(ik)^{2\alpha+1}}{(2\alpha+1)!} \bullet\!\!\!\vdots\, \alpha - 1 = \sum_{\alpha=1}^{\infty} \frac{(ik)^{2\alpha+1}}{(2\alpha+1)!} \left[ (4D\tau)^{1/2} (D\tau)^{\alpha} \frac{(2\alpha+1)!}{2(\alpha-1)!} \left( \sum_{j=2}^{n} c_j c_{j-1}^2 \right) \left( \sum_{j=1}^{n} c_j^2 \right)^{\alpha-1} \right] \\ &= -ik^3 (4D\tau)^{1/2} \beta_1 \exp(-\beta k^2),\end{aligned} \tag{18}$$

where $\beta = D\tau \sum_{j=1}^{n} c_j^2 \approx Dn\tau$ and $\beta_1 = D\tau \sum_{j=2}^{n} c_j c_{j-1}^2/2 \approx Dn\tau/2$ for $n \to \infty$. Again, the number $\alpha - 1$ is associated only with the trivial double tree. The Fourier transform of Eq. (18) yields

$$P_1^{(2)}(x_{n+1}) = (4D\tau)^{\frac{1}{2}} \frac{\beta_1 x_{n+1} \left( x_{n+1}^2 - 6\beta \right)}{8\beta^3} \frac{1}{\sqrt{4\pi\beta}} \exp\left( - \frac{x_{n+1}^2}{4\beta} \right). \tag{19}$$

At asymptotically large $n$, we found that the prefactor of the Gaussian diffusive term in Eq. (19) scales as

$$(4D\tau)^{\frac{1}{2}}\frac{\frac{1}{2}Dn\tau x_{n+1}\left(x_{n+1}^2-6Dn\tau\right)}{8D^3n^3\tau^3}\sim\frac{n\times n^{\frac{1}{2}}\times n}{n^3}\sim n^{-\frac{1}{2}}, \tag{20}$$

since $x_{n+1}\sim n^{1/2}$. Hence, we can express the first-order probability distribution function of the particle in the asymptotic regime (i.e., $n\to\infty$) as follows:

$$P_1^{(2)}(x_{n+1})=O(n^{-\frac{1}{2}})\frac{1}{\sqrt{4\pi\,Dn\tau}}\exp\left(-\frac{x_{n+1}^2}{4Dn\tau}\right). \tag{21}$$

The second-order contribution of the Feynman's graphs turns out to be more complicated. Its determination requires us to consider separately the second-order characteristic function of $N=2$, $N=3$, and $N\geqslant 4$. For $N=2$,

$\Gamma_2^{(2)}(k)$

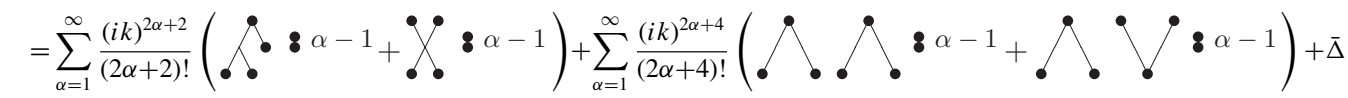


$$=4D\tau\left[(\beta_3-\beta_2)k^4-\frac{1}{2}\beta_1^2k^6\right]\exp(-\beta k^2); \tag{22}$$

for $N=3$,

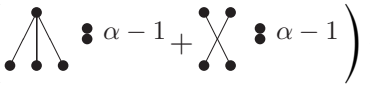


$$\Gamma_2^{(3)}(k)=\sum_{\alpha=1}^{\infty}\frac{(ik)^{2\alpha+2}}{(2\alpha+2)!}\left(\quad\bullet^{\alpha-1}+\quad\bullet^{\alpha-1}\right)+\bar{\Delta}=4D\tau[\beta_4k^4-\beta_2k^4]\exp(-\beta k^2); \tag{23}$$

and for $N\geqslant 4$,

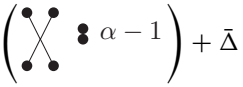


$$\Gamma_2^{(N\geqslant 4)}(k)=\sum_{\alpha=1}^{\infty}\frac{(ik)^{2\alpha+2}}{(2\alpha+2)!}\left(\quad\bullet^{\alpha-1}\right)+\bar{\Delta}=-4D\tau\beta_2k^4\exp(-\beta k^2), \tag{24}$$

with $\beta_2=D\tau\sum_{j=1}^{n}c_j^4/16\approx Dn\tau/16$, $\beta_3=D\tau\sum_{j=3}^{n}c_jc_{j-1}c_{j-2}^2/4\approx Dn\tau/4$, and $\beta_4=D\tau\sum_{j=2}^{n}c_jc_{j-1}^3/12\approx Dn\tau/12$, as $n\to\infty$. Note that $\bar{\Delta}$ accounts for error of order $O(n^{-1})$ made during the calculation of the zeroth- and first-order characteristic functions [41].

Taking the Fourier transforms of Eqs. (22), (23), and (24), the following probability distribution functions are obtained:

$$\begin{aligned}P_2^{(2)}(x_{n+1})=4D\tau\Bigg\{&\left[\frac{3(\beta_3-\beta_2)}{4\beta^2}-\frac{15\beta_1^2}{16\beta^3}\right]+\left[-\frac{3(\beta_3-\beta_2)}{4\beta^3}+\frac{45\beta_1^2}{32\beta^4}\right]x_{n+1}^2\\&+\left[\frac{\beta_3-\beta_2}{16\beta^4}-\frac{15\beta_1^2}{64\beta^5}\right]x_{n+1}^4+\frac{\beta_1^2}{128\beta^6}x_{n+1}^6\Bigg\}\frac{1}{\sqrt{4\pi\beta}}\exp\left(-\frac{x_{n+1}^2}{4\beta}\right),\end{aligned} \tag{25}$$

$$P_2^{(3)}(x_{n+1})=\frac{4D\tau}{16}\frac{\beta_4-\beta_2}{\beta^2}\left(12-\frac{12}{\beta}x_{n+1}^2+\frac{1}{\beta^2}x_{n+1}^4\right)\frac{1}{\sqrt{4\pi\beta}}\exp\left(-\frac{x_{n+1}^2}{4\beta}\right), \tag{26}$$

$$P_2^{(N\geqslant 4)}(x_{n+1})=-\frac{4D\tau}{16}\frac{\beta_2}{\beta^2}\left(12-\frac{12}{\beta}x_{n+1}^2+\frac{1}{\beta^2}x_{n+1}^4\right)\frac{1}{\sqrt{4\pi\beta}}\exp\left(-\frac{x_{n+1}^2}{4\beta}\right). \tag{27}$$

It is easy to observe that the prefactors of all these probability distribution functions scale as $O(n^{-1})$ when $n\to\infty$. Thus, combining Eqs. (25), (26), and (27), the second-order probability distribution function of the particle can be put in the following form:

$$P_2^{(N)}(x_{n+1})=O(n^{-1})\frac{1}{\sqrt{4\pi\,Dn\tau}}\exp\left(-\frac{x_{n+1}^2}{4Dn\tau}\right), \tag{28}$$

as $n\to\infty$.

Finally, according to Eqs. (17), (21), and (28), the asymptotic probability distribution function of the Brownian particle is given by

$$\begin{aligned}P^{(N)}(x_{n+1})=&\left[1+O(n^{-\frac{1}{2}})\delta_K(N,2)+O(n^{-1})\cdots\right]\\&\times\frac{1}{\sqrt{4\pi\,Dn\tau}}\exp\left(-\frac{x_{n+1}^2}{4Dn\tau}\right),\end{aligned} \tag{29}$$

which shows that the asymptotic convergence rate of $P^{(N\geqslant 3)}(x_{n+1})$ is of $O(n^{-1})$, while that of $P^{(2)}(x_{n+1})$ is of $O(n^{-1/2})$. This result signifies that chaotic fluctuations from Tchebyscheff maps of $N\geqslant 3$ brings about a faster convergence to the Gaussian diffusive limit than $N=2$. This

outcome is further validated through numerical simulations (see Fig. 1).

## IV. DETERMINISTIC SMOLUCHOWSKI-FEYNMAN RATCHET

A Smoluchowski-Feynman ratchet is the model of an overdamped Brownian particle in a spatially periodic and asymmetric potential being subjected to white Gaussian noise [1]. In this section, we shall construct a deterministic version by replacing the Gaussian noise with chaotic noise generated by the second-order Tchebyscheff map. We call this the deterministic Smoluchowski-Feynman ratchet.

Let us note that the spatially periodic asymmetric potential of our deterministic ratchet takes the following form:

$$V(x) = \frac{\mu}{c}\left(\sin \pi x + \frac{A}{4}\sin 2\pi x - d\right), \tag{30}$$

which is illustrated in Fig. 2. The parameters

$$c = \sin(\cos^{-1} u) + \frac{A}{4}\sin(2\cos^{-1} u) - d \tag{31}$$

and

$$d = \sin(2\pi - \cos^{-1} u) + \frac{A}{4}\sin(4\pi - 2\cos^{-1} u) \tag{32}$$

serve to normalize the potential and to set its minimum value to zero, respectively. Note that the variable

$$u = \frac{-1 + \sqrt{1 + 2A^2}}{2A},$$

except for $A = 0$ whereupon $u = 0$; and the maximum value of the potential is given by $\mu$. The parameter $A$ adjusts the asymmetry of the potential and its value will be restricted within the range $-2 \leqslant A \leqslant 2$. The period of the potential is 2.

The directed current $J_d$ of the dissipated Brownian particle which is acted by $-V'(x)$ and being kicked by chaotic noise from the second-order Tchebyscheff map can be determined from the following analytical expression [28]:

$$J_d = \left(\frac{\tau}{\gamma}\right)^{\frac{3}{2}} \frac{1}{Z}\int_{-1}^{1} V'(x) e^{\frac{-V(x)}{k_B T}} \left\{\int_{-1}^{x} G(x')dx' - W\int_{-1}^{x} e^{\frac{V(x')}{k_B T}} dx'\right\} dx, \tag{33}$$

where

$$Z = \int_{-1}^{1} e^{-\frac{V(x)}{k_B T}} dx, \tag{34}$$

$$G(x) = \frac{V''(x)}{(k_B T)^{1/2}} - \frac{V'(x)^2}{(k_B T)^{3/2}}, \tag{35}$$

and

$$W = \frac{\int_{-1}^{1} G(x)dx}{\int_{-1}^{1} e^{\frac{V(x)}{k_B T}} dx}. \tag{36}$$

Note that Eq. (33) is true under the condition $\tau/\gamma \ll 1$. It is a first-order perturbative result with respect to $\tau/\gamma$.

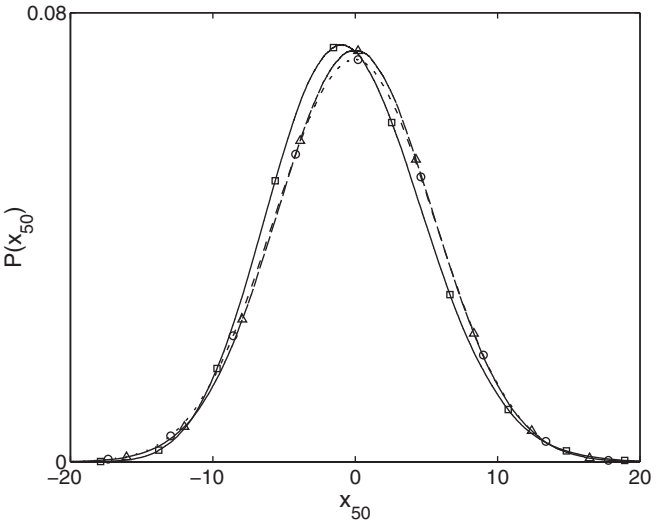


FIG. 1. The asymptotic probability distribution function of the particle based on numerical simulation for chaotic fluctuations from the $G^{(2)}$ map (solid curve with square markers), the $G^{(3)}$ map (dashed curve with triangle markers), and the $G^{(4)}$ map (dashed-dotted curve with circle markers). The parameters in dimensionless units are $\tau = 10.0, \gamma = 10.0, k_B T = 0.25$. The ensemble size used in the numerical simulation is $1 \times 10^5$, with an iteration length of 50.

A plot of $J_d$ versus the asymmetry factor $A$ based on Eq. (33), and that obtained by numerical simulation from the QKP map through

$$J_d = \lim_{n\to\infty} \frac{1}{n}\langle\langle x_{n-1} - x_0\rangle\rangle, \tag{37}$$

is shown in Fig. 3. The notation $\langle\langle\cdots\rangle\rangle$ denotes the ensemble average. In the simulation, we assume $p_0 = 0$ and $x_0 = 0$, while the initial value $F_0$ is selected randomly within the range $[-1,1]$ based on the uniform probability distribution. Our simulations have found that it is possible for $F_0$ to lie occasionally in the basin of attraction of the fixed point $F^* = 1$ of the map. When that happens, it is necessary to remove the

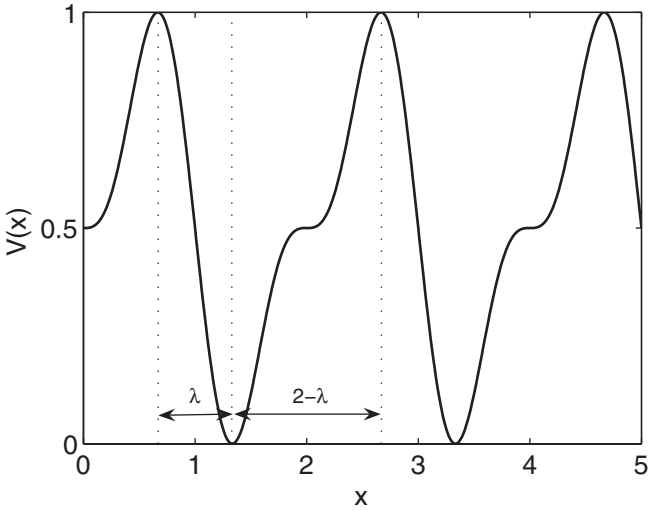


FIG. 2. The spatially periodic and asymmetric potential given by Eq. (30) with $\mu = 1$ and $A = -2$.

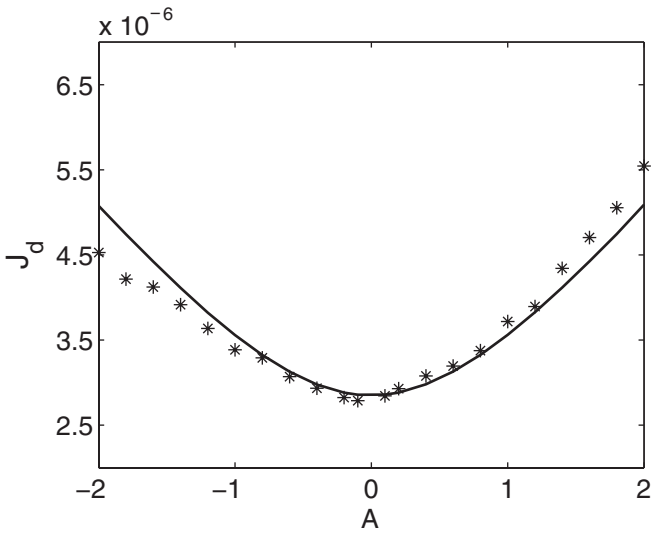


FIG. 3. The directed current $J_d$ against the asymmetric factor $A$ of the spatially periodic and asymmetric potential. The solid line represents analytical results from Eq. (33), while the $*$'s represents numerical solutions. The parameters in dimensionless units are $\tau = 1$, $\gamma = 2 \times 10^3$, $k_BT = 0.2$, $\mu = 1$. The ensemble size used in the simulation is $1 \times 10^3$, with an iteration length of $1 \times 10^7$.

corresponding trajectory from the ensemble in order to ensure that the underlying fluctuations that generate the motion of the Brownian particle is ergodic, which is our basic assumption on the characteristics of the chaotic noise.

As shown in Fig. 3, the transport of the particle is enhanced when the asymmetry of the spatially periodic potential is increased. However, the increase is not symmetrical between the positive and the negative values of $A$. While this is obvious in the numerical results, it is also true in the analytical results although the difference is slight. A better correspondence to the numerical results will occur if higher-order corrections are taken over the first-order results given by Eq. (33). However, these higher-order corrections will be too complicated to be useful for our purposes. The difference in transport behavior of the Brownian particle when the periodic potential assumes the factor $A$ and $-A$ can be understood based on the following reasons: (1) the statistical asymmetry of the noise leads to an unequal transition rate over the right and the left barrier, and (2) both the transition rates depend on the shape of its barrier.

## V. CONSTANT FLASHING DETERMINISTIC SMOLUCHOWSKI-FEYNMAN RATCHET

An approach to rectify the motion of the Brownian particle when the noise is Gaussian is to switch on and off the spatially periodic potential for a certain length of time. If the on time and off time occur at a fixed interval, the system is known as a constant flashing ratchet [1,4,13]. We can apply this on and off flashing of the potential to the QKP map and compare the transport of the Brownian particle when the noise is either Gaussian or chaotic. In the case of Gaussian noise, we simply replace $F_{n+1}$ of Eq. (2) by a Gaussian random variable of variance one and rescale the intensity of the noise such that $s = \sqrt{2k_BT}$. When the potential is turned off, the particle is expected to diffuse normally for both the Gaussian and the chaotic noise. This is so for the latter case if the noise were to arise from the Tchebyscheff maps and the turn off time is sufficiently long, based on our analysis in Sec. III. In other words, we expect the motion of the particle to obey the Gaussian diffusive process. When the potential is turned on, the particle is driven to the nearest potential minimum, and if the potential is asymmetric, there will be a net motion of the particle in the direction with the steeper slope. However, for the case of the chaotic noise, the motion of the particle is influenced by an additional component due to the directed current given by Eq. (33). If we were to assume that the particle diffuses within $\lambda$ or $2 - \lambda$ (see Fig. 2) within the turn off time, we arrive at a restriction on the number of iterates $n_{\rm off}$ when the potential is turned off [4]:

$$\frac{\gamma\kappa_{\rm min}}{2k_BT\tau} < n_{\rm off} < \frac{\gamma\kappa_{\rm max}}{2k_BT\tau}, \tag{38}$$

where $\kappa_{\rm min}$ and $\kappa_{\rm max}$ take the minimum and maximum value of the set $\{\lambda^2,(2-\lambda)^2\}$, respectively. This restriction suggests the following analytical expression for the directed current of Brownian particle in a constant flashing ratchet with chaotic noise:

$$J = \frac{\mathrm{erfc}\left(\frac{2-\lambda}{\sqrt{4Dn_{\rm off}\tau}}\right) - \mathrm{erfc}\left(\frac{\lambda}{\sqrt{4Dn_{\rm off}\tau}}\right) + J_d n_{\rm on}\tau}{(n_{\rm on}+n_{\rm off})\tau}. \tag{39}$$

Note that erfc is the complementary error function, and for constant flashing, we expect the number of iterates when the

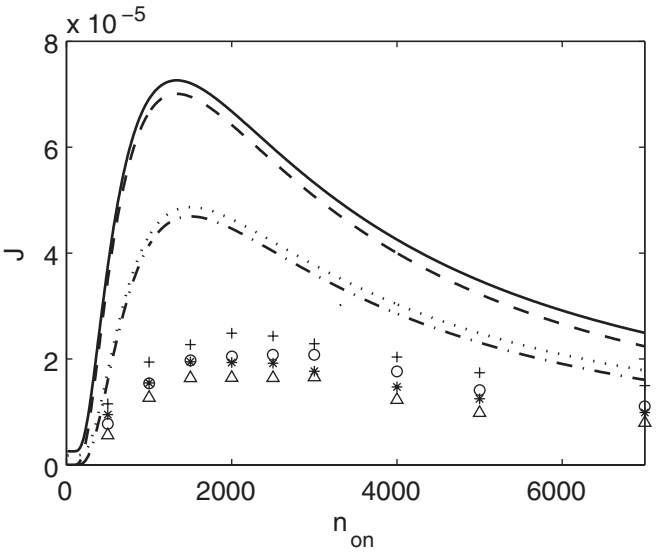


FIG. 4. The directed current $J$ versus the turn on time $n_{\rm on}$ of the constant flashing ratchet. We have assumed $n_{\rm on} = n_{\rm off}$. The curves from top to bottom are as follows: (solid line) analytical result, chaotic noise for $A = 2$; (dashed line) analytical result, Gaussian noise for $A = 2$; (dotted line) analytical result, chaotic noise for $A = 1$; (dash-dotted line) analytical result, Gaussian noise for $A = 1$; (+) numerical result, chaotic noise for $A = 2$; ($\circ$) numerical result, Gaussian noise for $A = 2$; ($*$) numerical result, chaotic noise for $A = 1$; and ($\triangle$) numerical result, Gaussian noise for $A = 1$. Note that the analytical results are given by Eq. (39), with $J_d = 0$ in the case of Gaussian noise. The parameters in dimensionless units are $\tau = 1$, $\gamma = 2 \times 10^3$, $k_BT = 0.2$, $\mu = 1$. The ensemble size used in the simulation is $1 \times 10^3$, with an iteration length of $1 \times 10^6$.

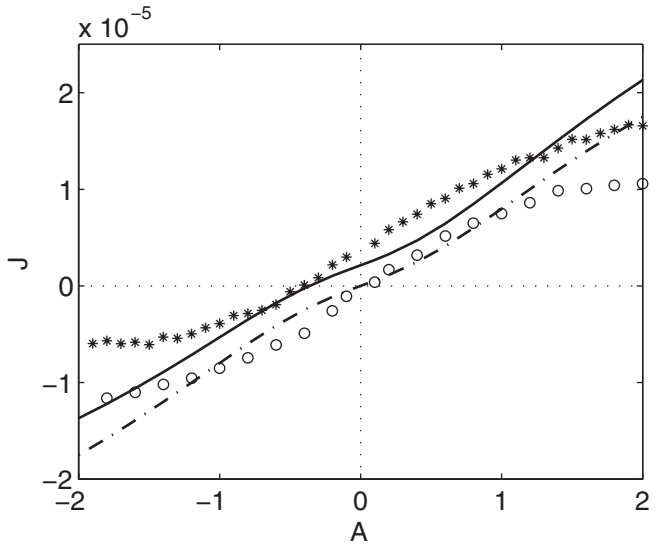


FIG. 5. A comparison of the relation between the directed current $J$ and the asymmetric factor $A$ for the constant flashing ratchet when $n_{\text{on}} = 1500$ and $n_{\text{off}} = 500$. The curves are given as follows: (solid line) analytical result for chaotic noise; (dash-dotted line) analytical result for Gaussian noise; (∗) numerical result for chaotic noise; and (○) numerical result for Gaussian noise. The analytical results are based on Eq. (39), with $J_d$ set to zero for the case of Gaussian noise. The parameters in dimensionless units are $\tau = 1, \gamma = 2 \times 10^3$, $k_B T = 0.2$, $\mu = 1$. The ensemble size used in the simulation is $1 \times 10^3$, with an iteration length of $1 \times 10^6$.

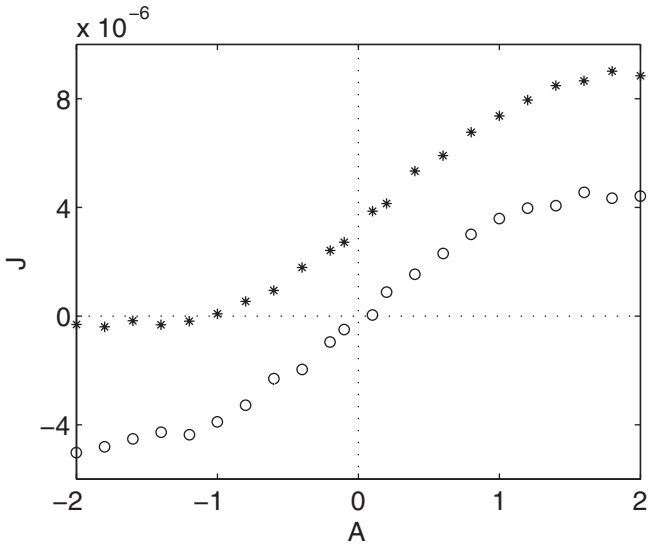


FIG. 6. A comparison of the relation between the directed current $J$ and the asymmetric factor $A$ for the dichotomous flashing ratchet. The curves are given as follows: (∗) numerical result for chaotic noise; and (○) numerical result for Gaussian noise. The parameters in dimensionless units are $\nu = 50$, $\varepsilon = 0.01$, $\tau = 1$, $\gamma = 2 \times 10^3$, $k_B T = 0.2$, $\mu = 1$. The ensemble size used in the simulation is $2 \times 10^3$, with an iteration length of $2 \times 10^6$.

potential is turned on $n_{\text{on}}$ and turned off $n_{\text{off}}$, to be constant for all time. If the chaotic noise were to arise from the second-order Tchebyscheff map, $J_d$ is to be obtained from Eq. (33).

Figure 4 illustrates the relation between the directed current $J$ of the constant flashing ratchet and the turn on time $n_{\text{on}}$ (or turn off time $n_{\text{off}}$ since we assume here that $n_{\text{on}} = n_{\text{off}}$) when the noise is either Gaussian or chaotic. We observe the expected convergence to zero for the current $J$ as $n_{\text{on}} \to 0$. However, for $n_{\text{on}} \to \infty$, we expect $J$ to vanish for the case of Gaussian noise and $J \to J_d/2$ for the case of chaotic noise. While we observe that increasing the asymmetry of the periodic potential in Gaussian noise enhances $J$, we found that driving the system further away from equilibrium through chaotic noise amplifies $J$ even further. The figure shows that the numerical results and the analytical results do not match each other. This is to be expected since the first two terms of the numerator of Eq. (39) have not taken into account the precise shape of the potential [4,13]. The more important observation is that both numerical and analytical results display the same trend, which support the mechanism of current generation as given by Eq. (39) for both the Gaussian and the chaotic noise. Nonetheless, our numerical simulations show that when $n_{\text{on}} = 1500$ and $n_{\text{off}} = 500$, the analytical and numerical results can closely correspond to each other. In this case, Eq. (39) serves as the empirical relation for the numerical results. This is shown in Fig. 5 which illustrates the relationship between $J$ and the asymmetric factor $A$ when the noise is Gaussian or chaotic. We again observe from the figure that the current is enhanced by a greater asymmetry of the potential. In addition, the chaotic noise is found again to further boost the current in the positive direction.

Let us next consider an example when the potential flashes on and off dichotomously. The state of the potential, which is either "on" or "off" as characterized by the random variable $\eta_n$ at the time instant $n$, now switches randomly between the two states in time. The rate of switching from the on state to the off state is $\varepsilon_{\text{on}}$ and from the off state to the on state is $\varepsilon_{\text{off}}$. The variable $\eta_n$ obeys the following statistic [48]:

$$\langle \eta_n \rangle = 0, \tag{40}$$

$$\langle \eta_n \eta_{n+\Delta n} \rangle = \exp\left( - \frac{|\Delta n|}{\nu} \right), \tag{41}$$

with $\nu = 1/(\varepsilon_{\text{on}} + \varepsilon_{\text{off}})$ being the correlation time of the dichotomous noise. Similar to the constant flashing case, we apply the dichotomous on and off flashing to the potential of the QKP map and investigate its effect on the directed transport of the Brownian particle driven either by Gaussian or chaotic noise. Note that we have assumed $\tau < \nu$. We have also assumed that the dichotomous noise is symmetric; that is, $\varepsilon_{\text{on}} = \varepsilon_{\text{off}} = \varepsilon$. Our result is displayed in Fig. 6, where we again observe an enhanced transport due to the chaotic noise in the positive direction. In Fig. 6, we also notice a shift in the point where the current vanishes. The occurrence of zero current at these points results from the restoration of the symmetry of detailed balance, which implies that the effect of statistical asymmetry has been neutralized. Note that this observation applies to Fig. 5, as well as Figs. 7 to 11 to be discussed later. For each of these cases, the compensation is performed through the tuning of some parameter in the system. In the case of Figs. 5 and 6, the parameter is the asymmetric factor $A$ of the potential.

## VI. RATCHET WITH STATE-DEPENDENT DIFFUSION IN CHAOTIC NOISE

In this section, we generalize our previous formulation and let the intensity of the chaotic noise $s$ to depend on $x$. With $s(x) = 2\sqrt{\gamma D(x)} = 2\sqrt{k_B T(x)}$, this is equivalent to the case when the Brownian particle is subjected to a state-dependent diffusion $D(x)$ [49]. Alternatively, we may presume the particle to be immersed in a "chaotic" heat bath with a spatially varying temperature $T(x)$. By inserting $s \to s(x_n)$ in Eq. (2) and assuming $\gamma\tau \gg 1$, we arrive at a simplified map relating the chaotic noise $F_n$ and the position variable $x_n$:

$$F_{n+1} = G(F_n), \tag{42}$$

$$x_{n+1} = x_n + \left(\frac{\tau}{\gamma}\right)^{1/2} s(x_n) F_n - \left(\frac{\tau}{\gamma}\right) V'(x_n). \tag{43}$$

Next, we apply the Perron-Frobenius approach [28] through the consideration of an ensemble of trajectories. We make the following perturbative ansatz on the probability density function $\rho(F,x,t)$:

$$\rho(F,x,t) = \rho^{(0)}(F,x,t) + \left(\frac{\tau}{\gamma}\right)^{1/2} q^{(1)}(F,x,t) + \left(\frac{\tau}{\gamma}\right) q^{(2)}(F,x,t) + O\left[\left(\frac{\tau}{\gamma}\right)^{3/2}\right]. \tag{44}$$

By performing a detailed calculation as before [28] and noting that the map $G$ is a complete map, we arrive at the following differential equation for the zeroth-order probability distribution $P_0(x,t)$:

$$\frac{\partial^2}{\partial x^2}[D(x)P_0(x,t)] + \frac{\partial}{\partial x}\left(\frac{V'(x)}{\gamma} P_0(x,t)\right) - \frac{\partial P_0(x,t)}{\partial t} = \frac{1}{\gamma}\frac{\partial}{\partial x}\int_{-1}^{1} dF\, F s(x)\, q^{(1)}(F,x,t). \tag{45}$$

Note that $P_0(x,t)$ is related to the zeroth-oder probability density function $\rho^{(0)}(F,x,t)$ as follows:

$$\rho^{(0)}(F,x,t) = h(F) P_0(x,t). \tag{46}$$

Equation (45) generalizes the Smoluchowski equation with a source term that we have obatined in [28] to the case of a spatially dependent diffusion $D(x)$. In this case, the source term is given by $(1/\gamma)\,\partial/\partial x \int_{-1}^{1} dF\, F s(x)\, q^{(1)}$.

If we were to restrict ourselves to a subclass of the complete map known as the double symmetric map, we can reduce Eq. (45) to the following homogeneous form:

$$\frac{\partial^2}{\partial x^2}[D(x)P_0(x,t)] + \frac{\partial}{\partial x}\left(\frac{V'(x)}{\gamma} P_0(x,t)\right) - \frac{\partial P_0(x,t)}{\partial t} = 0. \tag{47}$$

This restriction allows us to analyze the next order of the perturbative ansatz:

$$\rho^{(1)}(F,x,t) = \rho^{(0)}(F,x,t) + \left(\frac{\tau}{\gamma}\right)^{1/2} q^{(1)}(F,x,t) = h(F) P_1(x,t), \tag{48}$$

where

$$P_1(x,t) = P_0(x,t) + \left(\frac{\tau}{\gamma}\right)^{1/2} Q_1(x,t). \tag{49}$$

The analysis leads to the following generalized inhomogeneous Smoluchowski equation for the first-order position probability distribution $P_1(x,t)$ of the particle:

$$\frac{\partial^2}{\partial x^2}[D(x)P_1(x,t)] + \frac{\partial}{\partial x}\left(\frac{V'(x)}{\gamma} P_1(x,t)\right) - \frac{\partial P_1(x,t)}{\partial t} = \frac{\tau^{1/2}}{\gamma^{3/2}}\frac{\partial}{\partial x}\int_{-1}^{1} dF\, F s(x)\, q^{(2)}(F,x,t). \tag{50}$$

In order to determine a mathematical expression of the directed current, which occurs in the steady state, we set $\partial P_1/\partial t = 0$, and integrate Eq. (50) to get

$$\frac{d}{dx}[D(x)P_1(x)] + \frac{V'(x)}{\gamma} P_1(x) = I(x) - J_1, \tag{51}$$

where $J_1$ is a constant of integration and

$$I(x) = \frac{\tau^{1/2}}{\gamma^{3/2}} \int_{-1}^{1} dF\, F s(x)\, q^{(2)}(F,x). \tag{52}$$

Considering the specific case of the second-order Tchebyscheff map, which is a double symmetric map, we can determine the inhomogenous term $I(x)$ by means of the approach given in [28]. Our manipulation leads to

$$I(x) = \frac{\tau^{1/2}}{8\gamma^{3/2}} s(x) \frac{d^2}{dx^2}[s(x)^2 P_0(x)] = \sqrt{\tau D(x)}\, \frac{d^2}{dx^2}[D(x)P_0(x)]. \tag{53}$$

This requires us to solve for $P_0(x)$. Integrating Eq. (47) by means of the integrating factor $\exp[\psi(x)]$ with

$$\psi(x) = \int_{-1}^{x} \frac{V'(x')}{\gamma D(x')} dx', \tag{54}$$

we obtain

$$P_0(x) = \frac{e^{-\psi(x)}}{D(x)}\left(N_0 - J_0 \int_{-\infty}^{x} e^{\psi(y)} dy\right), \tag{55}$$

where $N_0$ and $J_0$ are constants of integration. $\psi(x)$ is known as the generalized potential.

We consider the situation where the potential $V(x)$ and the diffusion $D(x)$ are spatially periodic with a period of 2; that is,

$$V(x+2n) = V(x), \tag{56}$$

$$D(x+2n) = D(x). \tag{57}$$

These conditions imply that

$$P_0(x+2n) = P_0(x) \tag{58}$$

and

$$\psi(x) - \psi(x+2) = 2\Delta. \tag{59}$$

Employing these results, we obtain $N_0 = 0$. With $\int_{-1}^{1} P_0(x)dx = 1$, we yield

$$J_0 = \frac{1 - e^{-2\Delta}}{\int_{-1}^{1} dx \frac{e^{-\psi(x)}}{D(x)} \int_{x}^{x+2} dy e^{\psi(y)}}. \tag{60}$$

This leads to

$$P_0(x) = \frac{1}{Z_0} \frac{e^{-\psi(x)}}{D(x)} \int_{x}^{x+2} e^{\psi(y)} dy, \tag{61}$$

where

$$Z_0 = \int_{-1}^{1} dx \frac{e^{-\psi(x)}}{D(x)} \int_{x}^{x+2} e^{\psi(y)} dy. \tag{62}$$

Putting these results into Eq. (53), we arrive at the following expression for the inhomogeneous term:

$$I(x) = -\frac{\sqrt{\tau D(x)}}{\gamma Z_0} \left\{ \left( V''(x) - \frac{V'(x)^2}{\gamma D(x)} - \frac{V'(x)D'(x)}{D(x)} \right) \times \frac{e^{-\psi(x)}}{D(x)} \int_{x}^{x+2} e^{\psi(y)} dy + \frac{V'(x)}{D(x)} (e^{-2\Delta} - 1) \right\}. \tag{63}$$

Equation (63) implies that

$$I(x + 2n) = I(x). \tag{64}$$

In the same vein, we can solve for $P_1(x)$ by integrating Eq. (51) with the integrating factor $\exp[\psi(x)]$. The result is

$$P_1(x) = \frac{e^{-\psi(x)}}{D(x)} \left( \int_{-1}^{x} I(x') e^{\psi(x')} dx' - J_1 \int_{-1}^{x} e^{\psi(x')} dx' + N_1 \right), \tag{65}$$

with $N_1$ being the second constant of integration. By employing the periodicity condition

$$P_1(x + 2n) = P_1(x) \tag{66}$$

and the normalization condition

$$\int_{-1}^{1} P_1(x)dx = 1, \tag{67}$$

it is easy to show that the first constant of integration

$$J_1 = \frac{1}{Z_0} \left[ \int_{-1}^{1} dx \frac{e^{-\psi(x)}}{D(x)} \int_{x}^{x+2} dx' I(x') e^{\psi(x')} + (1 - e^{-2\Delta}) \right]. \tag{68}$$

With $J_1$ determined, $N_1$ is determined through the normalization condition Eq. (67):

$$N_1 = \frac{1}{\int_{-1}^{1} \frac{e^{-\psi(x')}}{D(x')} dx'} \left\{ 1 - \int_{-1}^{1} \frac{e^{-\psi(x)}}{D(x)} dx \left( \int_{-1}^{x} I(x') e^{\psi(x')} dx' - J_1 \int_{-1}^{x} e^{\psi(x')} dx' \right) \right\}. \tag{69}$$

The analytical expression of the directed current is then obtained by inserting the above fully determined Eq. (65) into the following equation:

$$J_d = -\left( \frac{\tau}{\gamma} \right) \int_{-1}^{1} V'(x) P_1(x) dx. \tag{70}$$

Let us now consider the specific case of a potential $V(x)$ that is asymmetric and spatially periodic as given by Eq. (30). Furthermore, we assume the state-dependent diffusion to take the following form:

$$\frac{1}{D(x)} = \frac{1}{D_0} [1 - \epsilon \cos(\pi x - \phi)], \tag{71}$$

where $\epsilon$ and $\phi$ are the amplitude and phase of the modulation. The amplitude $\epsilon$ is restricted to the range $0 \leqslant \epsilon < 1$, and $D_0$ is a positive constant. By means of Eq. (54), we obtain the following explicit expression for the generalized potential:

$$\psi(x) = \frac{\mu\pi}{\gamma c D_0} \left\{ \frac{1}{\pi} \sin(\pi x) + \frac{A}{4\pi} \sin(2\pi x) - \epsilon \left[ \frac{1}{4\pi} \sin(2\pi x - \phi) + \frac{x}{2} \cos(\phi) + \frac{A}{12\pi} \sin(3\pi x - \phi) + \frac{A}{4\pi} \sin(\pi x + \phi) \right] \right\}. \tag{72}$$

Note that we have ignored an arbitrary constant in the above equation since it will be canceled off in subsequent calculation. From Eqs. (59) and (72), we obtain

$$\Delta = \frac{\mu\pi\epsilon \cos(\phi)}{2c\gamma D_0}. \tag{73}$$

Substituting Eqs. (71) to (73) as well as Eq. (30) into Eqs. (63), (65), (68), and (69), we then obtain the directed current $J_d$ through the analytical expression given by Eq. (70). The directed current $J_d$ can also be calculated numerically through Eqs. (1) to (3) with $s$ replaced with $s(x)$ and employing Eq. (37). We first plot $J_d$ against the phase $\phi$ in Fig. 7 for $A = 0$, that is, the potential is spatially symmetric and periodic, with results obtained from these two approaches. We find

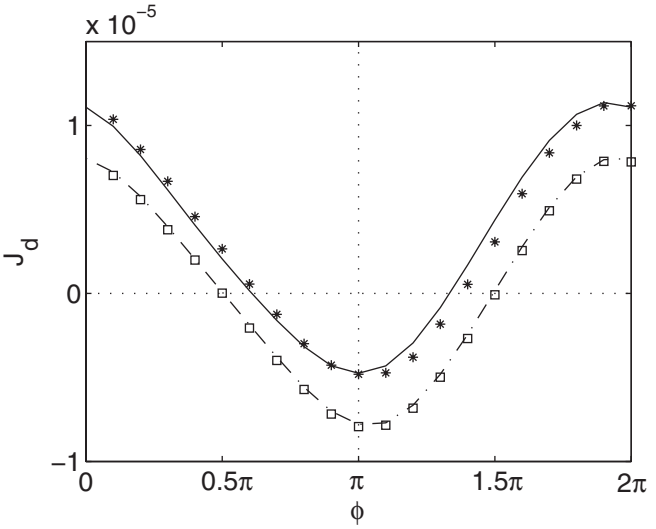


FIG. 7. The directed current $J_d$ versus the phase $\phi$ of the state dependent diffusion. The potential is spatially periodic and symmetric; that is, $A = 0$. The curves are as follows: (solid line) analytical results for chaotic noise; (∗) numerical results for chaotic noise; (dash-dotted line) analytical results for Gaussian noise; and (□) numerical results for Gaussian noise. The parameters in dimensionless units are $\tau = 1$, $\gamma = 2 \times 10^3$, $k_B T = 0.2$, $\mu = 1$, $\epsilon = 0.2$. The ensemble size used in the simulation is $1 \times 10^3$, with an iteration length of $1 \times 10^7$.

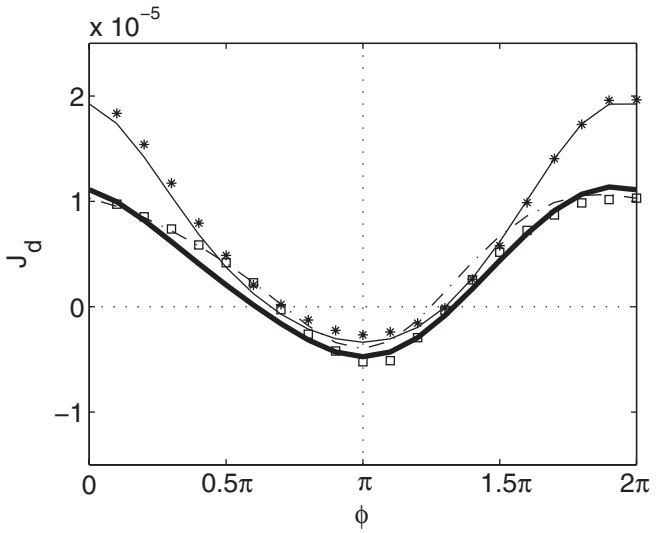


FIG. 8. The directed current $J_d$ versus the phase $\phi$ of the state dependent diffusion for the case of chaotic noise. The solid line in Fig. 7 has been replotted here as a thick solid line for the purpose of comparison. The rest of the curves are as follows: (dash-dotted line) analytical results for $A = -2$; (□) numerical results for $A = -2$; (thin solid line) analytical results for $A = 2$; and (∗) numerical results for $A = 2$. The details of the simulation parameters employed are the same as those used in Fig. 7.

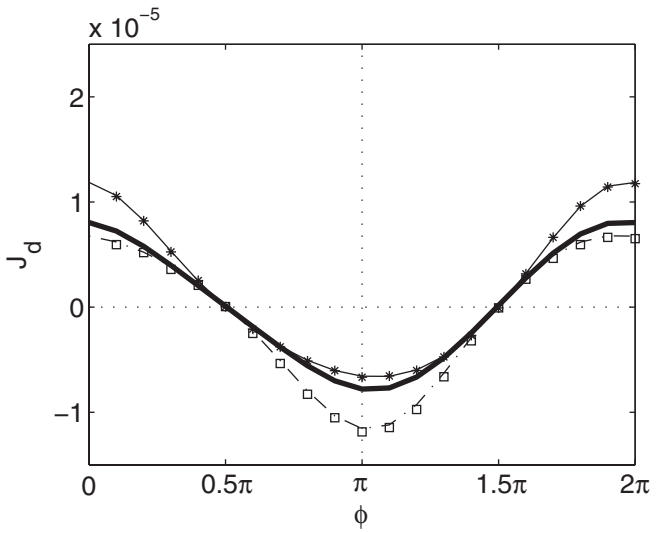


FIG. 9. The directed current $J_d$ versus the phase $\phi$ of the state dependent diffusion for the case of Gaussian noise. The dash-dotted line in Fig. 7 has been replotted here as a thick solid line for the purpose of comparison. The rest of the curves are as follows: (dash-dotted line) analytical results for $A = -2$; (□) numerical results for $A = -2$; (thin solid line) analytical results for $A = 2$; and (∗) numerical results for $A = 2$. The details of the simulation parameters employed are the same as those used in Fig. 7.

close correspondence between our analytical and numerical results. It is instructive to compare these results to the case when the noise is Gaussian. For Gaussian noise, the analytical expression of the directed current is given by

$$J_d = -\left(\frac{\tau}{\gamma}\right)\int_{-1}^{1} V'(x)P_0(x)dx, \tag{74}$$

with $P_0(x)$ given by Eq. (61). On the other hand, the numerical results are determined through Eqs. (1) to (3) with $F_{n+1}$ of Eq. (2) replaced by a Gaussian random variable of variance one such that $s(x) = \sqrt{2k_BT(x)}$. Again, we observe both the analytical and the numerical results to correspond closely to each other. When we compare the directed current between the systems driven by the chaotic and the Gaussian noise, we notice that the statistical asymmetry in the chaotic noise (which is generated from the second-order Tchebyscheff map) has biased the current toward the positive direction. As we turn on the asymmetry of the potential, we observe a further increase of the directed current in the positive direction when the noise is chaotic (see Fig. 8). This is consistent with the results shown in Fig. 3. The combined effect of the statistical asymmetry of the noise and the spatial asymmetry of the potential on the directed current can be understood through Fig. 9. Figure 9 shows how the presence of asymmetry in the potential alone can enhance the directed current, since the Gaussian noise is statistically symmetric. Thus, we see that statistical asymmetry has the effect of raising the current curves in Fig. 9 to give rise to the corresponding curves in Fig. 8. In other words, statistical asymmetry provides an extra push to the directed current in the positive direction.

## VII. TILTED DETERMINISTIC SMOLUCHOWSKI-FEYNMAN RATCHET

In this section, we include a tilt in the deterministic Smoluchowski-Feynman ratchet through the addition of a homogeneous static load force $F_L$. We call this the tilted deterministic Smoluchowski-Feynman ratchet. We can apply the results in the last section to analyze the directed transport in this ratchet system. To begin, let us note that the potential now takes the following form:

$$V(x) = \frac{\mu}{c}\left(\sin\pi x + \frac{A}{4}\sin 2\pi x - d\right) - xF_L, \tag{75}$$

with $c$ and $d$ defined in Eqs. (31) and (32), respectively. With the diffusion coefficient of the Smoluchowski-Feynman ratchet being a constant, we have $D = k_BT/\gamma$. By means of Eq. (54), we obtain the generalized potential as follows:

$$\psi(x) = \frac{1}{k_BT}\left(\frac{\mu}{c}\sin(\pi x) + \frac{A\mu}{4c}\sin(2\pi x) - xF_L\right), \tag{76}$$

which leads to

$$\Delta = \frac{F_L}{k_BT}. \tag{77}$$

With Eqs. (76) and (77), we can determine the directed current of the tilted deterministic Smoluchowski-Feynman ratchet based on the analytical expression given by Eq. (70). Conversely, the directed current can also be determined numerically through the QKP map by employing Eq. (75) as the potential force field. For the sake of comparison, we have also evaluated the current from the tilted Smoluchowski-Feynman ratchet [1]. This is obtained analytically from Eq. (74), and numerically through the QKP map by replacing the chaotic

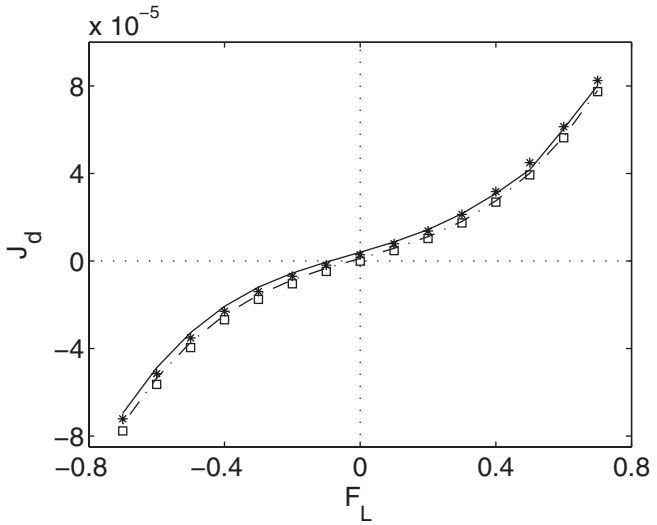


FIG. 10. The directed current $J_d$ versus the load $F_L$. The potential is spatially periodic and symmetric; that is, $A = 0$. The curves are as follows: (solid line) analytical results for chaotic noise; (∗) numerical results for chaotic noise; (dash-dotted line) analytical results for Gaussian noise; and (□) numerical results for Gaussian noise. The parameters in dimensionless units are $\tau = 1, \gamma = 2 \times 10^3$, $k_B T = 0.2$, $\mu = 1$. The ensemble size used in the simulation is $1 \times 10^3$, with an iteration length of $1 \times 10^7$.

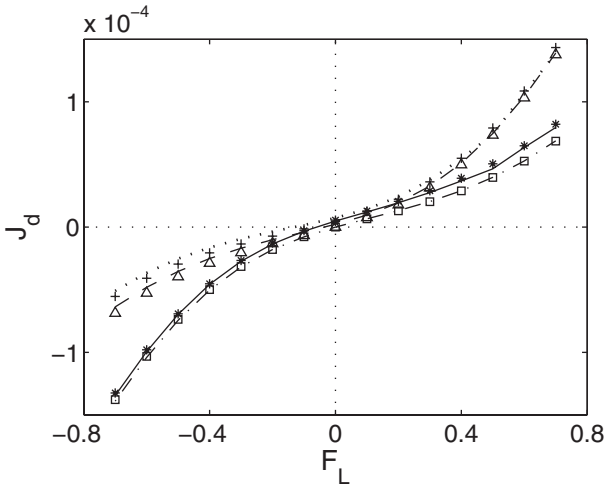


FIG. 11. The directed current $J_d$ versus the load $F_L$. The potential is spatially periodic and asymmetric. The curves are as follows: (dotted line) analytical results for chaotic noise with $A = -2$; (+) numerical results for chaotic noise with $A = -2$; (dashed line) analytical results for Gaussian noise with $A = -2$; (△) numerical results for Gaussian noise with $A = -2$; (solid line) analytical results for chaotic noise with $A = 2$; (∗) numerical results for chaotic noise with $A = 2$; (dash-dotted line) analytical results for Gaussian noise with $A = 2$; and (□) numerical results for Gaussian noise with $A = 2$. The details of the simulation parameters employed are the same as those used in Fig. 10.

noise with the Gaussian noise in the manner discussed in the last section.

Let us now analyze the transport behavior of the tilted deterministic Smoluchowski-Feynman ratchet. First, note that the presence of the constant load force causes the potential to tilt to the right when $F_L > 0$ and left when $F_L < 0$. In the absence of spatial asymmetry and statistical asymmetry, that is, $A = 0$ and the noise is Gaussian, we expect such a tilted ratchet to produce a positive current for $F_L > 0$ and negative current for $F_L < 0$. More precisely, the current should be antisymmetric about the origin as shown in Fig. 10. However, this symmetry is broken by the statistical asymmetry that is inherent within the chaotic noise generated from the second-order Tchebyscheff map, which leads to a positive shift in the current as shown in Fig. 10. The symmetry can also be broken by the sole effect of spatial asymmetry as illustrated in Fig. 11 for the case of Gaussian noise. In this case, the Brownian particle faces either a shallower or a steeper slope as it travels downhill, which corresponds to an enhanced current in the former case and a diminished current in the latter case. Since the particle faces a different slope for $F_L > 0$ and $F_L < 0$, this explains the asymmetry in the current for the Gaussian noise. Now, if we were to put in the chaotic noise, there is the additional effect of statistical asymmetry, which leads to a positive shift of the respective directed currents of the Gaussian noise for $A = -2$ and $A = 2$, as demonstrated in Fig. 11. Thus, the breaking of a geater number of symmetries seems to have the effect of creating a larger directed current.

## VIII. DISCUSSION AND CONCLUSION

In this paper, we have employed the chaotic noise generated by the second-order Tchebyscheff map as the "heat source" for the deterministic Smoluchowski-Feynman ratchets. There is no loss of generality in this choice as chaotic noise from higher even-order Tchebyscheff maps should produce similar results on directed transport as those produced by the second-order Tchebyscheff map, albeit with a smaller current due to a smaller statistical asymmetric effect. On the other hand, we expect the results for the odd-order Tchebyscheff maps to be the same as those obtained from the Gaussian noise, since all the odd higher-order correlations vanish for both kinds of noise [28,36].

In addition to statistical asymmetry, we have also introduced asymmetry into the spatially periodic potential force field. For the zero mean deterministic ratchets considered in this paper, these two forms of asymmetries are the source of the directed current. Indeed, a proper exploitation of these two asymmetries is necessary to create and to enhance the size of the directed current. For example, it is well known that potential asymmetry alone is not able to create a current in the Smoluchowski-Feynman ratchet. We showed that by adding statistical asymmetry, a current can flow in the deterministic Smoluchowski-Feynman ratchet. In fact, the more asymmetric is the potential force field, the larger is the size of this current. The size of the current can also be enhanced by using the right type of deterministic Smoluchowski-Feynman ratchets. For example, a larger current can be obtained from the constant flashing or the state-dependent deterministic Smoluchowski-Feynman ratchet studied in this paper. These ratchets are already known to produce current in Gaussian noise. The effect of statistical asymmetry is to drive these systems even further away from thermodynamic equilibrium, causing an enhancement in the directed current.

In conclusion, we have investigated into deterministic Smoluchowski-Feynman ratchets which are driven by chaotic noise generated by the second-order Tchebyscheff map. Based on the inhomogeneous Smoluchowski equation and its generalized version, we are able to yield the analytical expression of the directed current of various deterministic Smoluchowski-Feynman ratchets. In particular, the source term of the inhomogeneous Smoluchowski equation indicates that the effect of statistical asymmetry is the cause of directional bias in the transport of the Brownian particle. This phenomenon is indeed observed for the deterministic Smoluchowski-Feynman ratchets considered in this paper, where analytical and numerical results are found to correspond closely with each other. In addition, we perceive that this phenomenon can be exploited to guide the design of real physical systems, such as the Brownian rectifiers and molecular sorters, in enhancing their efficiency and effectiveness for particle separation and segregation.


[1] P. Reimann, Phys. Rep. **361**, 57 (2002).
[2] M. O. Magnasco, Phys. Rev. Lett. **71**, 1477 (1993).
[3] M. O. Magnasco, Phys. Rev. Lett. **72**, 2656 (1994).
[4] R. D. Astumian and M. Bier, Phys. Rev. Lett. **72**, 1766 (1994).
[5] C. R. Doering, W. Horsthemke, and J. Riordan, Phys. Rev. Lett. **72**, 2984 (1994).
[6] A. Gomez-Marin and J. M. Sancho, Europhys. Lett. **86**, 40002 (2009).
[7] A. Gomez-Marin and J. M. Sancho, Phys. Rev. E **77**, 031108 (2008).
[8] R. D. Astumian, Phys. Rev. E **79**, 021119 (2009).
[9] A. Grimm, H. Stark, and J. R. C. van der Maarel, Phys. Rev. E **79**, 061102 (2009).
[10] M. Borromeo and F. Marchesoni, Phys. Rev. Lett. **99**, 150605 (2007).
[11] J. C. T. Eijkel and A. van den Berg, Electrophoresis **27**, 677 (2006).
[12] B. Q. Ai, Y. F. He, and W. R. Zhong, Phys. Rev. E **83**, 051106 (2011).
[13] R. D. Astumian, Science **276**, 917 (1997).
[14] A. V. Arzola, K. Volke-Sepúlveda, and J. L. Mateos, Phys. Rev. Lett. **106**, 168104 (2011).
[15] U. E. Vincent, A. Kenfack, D. V. Senthilkumar, D. Mayer, and J. Kurths, Phys. Rev. E **82**, 046208 (2010).
[16] K. Loutherback, J. Puchalla, R. H. Austin, and J. C. Sturm, Phys. Rev. Lett. **102**, 045301 (2009).
[17] H. Chen, Q. Wang, and Z. Zheng, Phys. Rev. E **71**, 031102 (2005).
[18] I. Zapata, S. Albaladejo, J. M. R. Parrondo, J. J. Sáenz, and F. Sols, Phys. Rev. Lett. **103**, 130601 (2009).
[19] F. Family, H. A. Larrondo, D. G. Zarlenga, and C. M. Arizmendi, J. Phys. Condens. Matter **17**, S3719 (2005).
[20] Q. Guo, S. M. McFaul, and H. Ma, Phys. Rev. E **83**, 051910 (2011).
[21] R. Salgado-García, M. Aldana, and G. Martínez-Mekler, Phys. Rev. Lett. **96**, 134101 (2006).
[22] R. Salgado-García, G. Martínez-Mekler, and M. Aldana, Phys. Rev. E **78**, 011126 (2008).
[23] P. Jung, J. G. Kissner, and P. Hänggi, Phys. Rev. Lett. **76**, 3436 (1996).
[24] J. L. Mateos, Phys. Rev. Lett. **84**, 258 (2000).
[25] J. H. Li and J. Łuczka, Phys. Rev. E **82**, 041104 (2010).
[26] S. Flach, O. Yevtushenko, and Y. Zolotaryuk, Phys. Rev. Lett. **84**, 2358 (2000).
[27] O. Farago and Y. Kantor, Phys. A **249**, 151 (1998).
[28] L. Y. Chew and C. Ting, Phys. Rev. E **69**, 031103 (2004).
[29] C.-H. Chang, Phys. Rev. E **66**, 015203(R) (2002).
[30] T. Hondou and Y. Sawada, Phys. Rev. Lett. **75**, 3269 (1995).
[31] D. R. Chialvo, M. I. Dykman, and M. M. Millonas, Phys. Rev. Lett. **78**, 1605 (1997).
[32] O. Yevtushenko, S. Flach, and K. Richter, Phys. Rev. E **61**, 7215 (2000).
[33] O. Yevtushenko, S. Flach, Y. Zolotaryuk, and A. A. Ovchinnikov, Europhys. Lett. **54**, 141 (2001).
[34] C. Beck, Physica A **169**, 324 (1990).
[35] L. Y. Chew and C. Ting, Physica A **307**, 275 (2002).
[36] L. Y. Chew, C. Ting, and C. H. Lai, Phys. Rev. E **72**, 036222 (2005).
[37] D. S. Goldobin, J.-N. Teramae, H. Nakao, and G. B. Ermentrout, Phys. Rev. Lett. **105**, 154101 (2010).
[38] H. Nakao, J.-N. Teramae, D. S. Goldobin, and Y. Kuramoto, Chaos **20**, 033126 (2010).
[39] P. Hänggi, R. Bartussek, P. Talkner, and J. Łuczka, Europhys. Lett. **35**, 315 (1996).
[40] C. Beck, Commun. Math. Phys. **130**, 51 (1990).
[41] A. Hilgers and C. Beck, Physica D **156**, 1 (2001).
[42] C. Beck, Physica A **233**, 419 (1996).
[43] P. Reimann, Phys. Rev. Lett. **86**, 4992 (2001).
[44] H. Kantz, W. Just, N. Baba, K. Gelfert, and A. Riegert, Physica D **187**, 200 (2004).
[45] H. Kantz and E. Olbrich, Physica A **253**, 105 (1998).
[46] C. Beck, Nonlinearity **4**, 1131 (1991).
[47] R. D. Mattuck, *A Guide to Feynman Diagrams in the Many-Body Problem* (McGraw-Hill, New York, 1976).
[48] D. Barik, P. K. Ghosh, and D. S. Ray, J. Stat. Mech (**2006**) P03010.
[49] M. Büttiker, Z. Phys. B Condens. Matter **68**, 161 (1987).